NASA/TM—2009-215593

A Kalman Approach to Lunar Surface Navigation Using Radiometric and Inertial Measurements

David T. Chelmins, Bryan W. Welch, O. Scott Sands, and Binh V. Nguyen
Glenn Research Center, Cleveland, Ohio

June 2009

NASA STI Program . . . in Profile

Since its founding, NASA has been dedicated to the advancement of aeronautics and space science. The NASA Scientific and Technical Information (STI) program plays a key part in helping NASA maintain this important role.

The NASA STI Program operates under the auspices of the Agency Chief Information Officer. It collects, organizes, provides for archiving, and disseminates NASA's STI. The NASA STI program provides access to the NASA Aeronautics and Space Database and its public interface, the NASA Technical Reports Server, thus providing one of the largest collections of aeronautical and space science STI in the world. Results are published in both non-NASA channels and by NASA in the NASA STI Report Series, which includes the following report types:

- TECHNICAL PUBLICATION. Reports of completed research or a major significant phase of research that present the results of NASA programs and include extensive data or theoretical analysis. Includes compilations of significant scientific and technical data and information deemed to be of continuing reference value. NASA counterpart of peer-reviewed formal professional papers but has less stringent limitations on manuscript length and extent of graphic presentations.

- TECHNICAL MEMORANDUM. Scientific and technical findings that are preliminary or of specialized interest, e.g., quick release reports, working papers, and bibliographies that contain minimal annotation. Does not contain extensive analysis.

- CONTRACTOR REPORT. Scientific and technical findings by NASA-sponsored contractors and grantees.

- CONFERENCE PUBLICATION. Collected papers from scientific and technical conferences, symposia, seminars, or other meetings sponsored or cosponsored by NASA.

- SPECIAL PUBLICATION. Scientific, technical, or historical information from NASA programs, projects, and missions, often concerned with subjects having substantial public interest.

- TECHNICAL TRANSLATION. English-language translations of foreign scientific and technical material pertinent to NASA's mission.

Specialized services also include creating custom thesauri, building customized databases, organizing and publishing research results.

For more information about the NASA STI program, see the following:

- Access the NASA STI program home page at *http://www.sti.nasa.gov*

- E-mail your question via the Internet to *help@sti.nasa.gov*

- Fax your question to the NASA STI Help Desk at 301–621–0134

- Telephone the NASA STI Help Desk at 301–621–0390

- Write to:
  NASA Center for AeroSpace Information (CASI)
  7115 Standard Drive
  Hanover, MD 21076–1320

NASA/TM—2009-215593

A Kalman Approach to Lunar Surface Navigation Using Radiometric and Inertial Measurements

David T. Chelmins, Bryan W. Welch, O. Scott Sands, and Binh V. Nguyen
Glenn Research Center, Cleveland, Ohio

National Aeronautics and
Space Administration

Glenn Research Center
Cleveland, Ohio 44135

June 2009

This report is a formal draft or working paper, intended to solicit comments and ideas from a technical peer group.

This report contains preliminary findings, subject to revision as analysis proceeds.

Level of Review: This material has been technically reviewed by technical management.

Available from

NASA Center for Aerospace Information
7115 Standard Drive
Hanover, MD 21076–1320

National Technical Information Service
5285 Port Royal Road
Springfield, VA 22161

Available electronically at http://gltrs.grc.nasa.gov

A Kalman Approach to Lunar Surface Navigation Using Radiometric and Inertial Measurements

David T. Chelmins, Bryan W. Welch, O. Scott Sands, and Binh V. Nguyen
National Aeronautics and Space Administration
Glenn Research Center
Cleveland, Ohio 44135

Summary

Future lunar missions supporting the NASA Vision for Space Exploration will rely on a surface navigation system to determine astronaut position, guide exploration, and return safely to the lunar habitat. In this report, we investigate one potential architecture for surface navigation, using an extended Kalman filter to integrate radiometric and inertial measurements. We present a possible infrastructure to support this technique, and we examine an approach to simulating navigational accuracy based on several different system configurations. The results show that position error can be reduced to 1 m after 5 min of processing, given two satellites, one surface communication terminal, and knowledge of the starting position to within 100 m.

Introduction

The NASA Vision for Space Exploration, announced by President Bush in 2004, calls for the safe return of astronauts to the Moon by 2020. NASA is investigating new methods of positioning and navigation that will facilitate exploration of the lunar surface. On Earth, the Global Positioning System (GPS) allows its users to quickly determine their locations and to plot courses of travel (Ref. 1). However, the Moon does not have the extensive satellite network required to duplicate terrestrial GPS. Even simple, compass-based methods are ineffective on the lunar surface because of the lack of a strong, central magnetic field. Therefore, new techniques for navigation, different from those used in terrestrial practice, must be developed for lunar surface missions.

The advancement of technology since the Apollo era allows electronics with reduced size, weight, and power (SWaP) to be integrated into the extravehicular activity (EVA) spacesuit. Previously, astronauts performing EVA relied on the Lunar Roving Vehicle for navigation because of the large SWaP requirements of the gyroscopes and computers used to make position determinations (Ref. 2). Now, it is feasible to install lightweight radio receivers, inertial measurement units (IMUs), and embedded processors to perform navigation calculations directly in the astronaut's suit. Besides adding convenience, suit-based navigation provides an extra measure of safety by allowing astronauts to return to the lunar lander in the event of Lunar Roving Vehicle failure. This capability is necessary under preliminary Constellation Program requirements, which define a navigational range of 10 km to walk back to the lunar habitat (Ref. 3).

The purpose of this study was to evaluate the performance of a lunar surface navigation system that uses radiometric and inertial techniques (Fig. 1). In the simulation, radiometric measurement capability is provided by two Lunar Relay Satellites (LRSs) and a surface Lunar Communication Terminal (LCT). Inertial measurements, used to determine three-dimensional acceleration, are delivered through an on-suit IMU. An extended Kalman filter (EKF) processes the data collected by both the radiometric and inertial methods and generates a dynamic position fix that provides navigation capability (Ref. 4). We expect that this approach, integrating radiometric and inertial measurements, will help overcome problems associated with each individual system, such as a slow update rate for radiometrics and long-term acceleration bias drift for IMUs (Ref. 5).

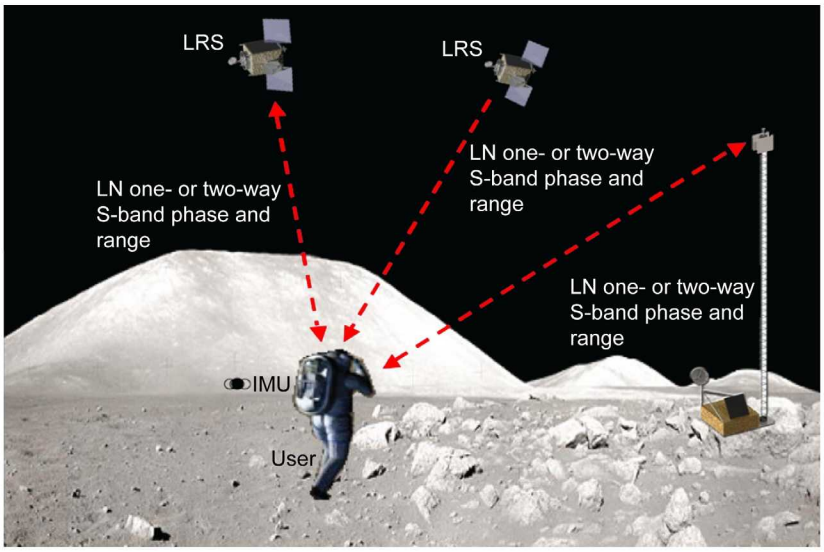

Figure 1.—Simulated lunar navigation (LN) concept. LRS, Lunar Relay Satellite; IMU, inertial measurement unit.

The EKF-based navigation method that we are applying has been used in similar terrestrial situations. GPS receivers are subject to periodic outages when satellite signals are obstructed by terrain features, such as tunnels or tall buildings. An approach taken in Reference 6 utilizes a Kalman filter to integrate an IMU with a GPS receiver. The IMU is calibrated continuously by radiometrics when available, and then it is used as a "flywheel" when a GPS outage occurs. Provided the outage is corrected quickly, IMU drift is minimized and the navigation system operates with relative accuracy. A similar product for vehicle land navigation is presented in Reference 7, where a 15-state Kalman filter processes GPS, IMU, and odometer data. A bank of Kalman filters is used in Reference 8 to detect and isolate GPS satellite failures while preserving prior measurements and position error estimates. The system integrates radiometrics, pressure altitude readings, and inertial data to allow aircraft to maintain a high level of confidence in airspace position.

This report presents one approach to a potential architecture for a lunar surface navigation system that couples radiometrics and inertial measurements. While reviewing the theoretical basis for the code, we discuss a MATLAB program used to simulate the accuracy of the architecture. Simulation results are provided for several potential system configurations and situations, and conclusions are drawn based on the position accuracy. Symbols are defined in the appendix to aid the reader.

Lunar Navigation Architecture

The space communication architecture for lunar surface operations has not yet been defined (Ref. 9). However, it is likely that one or two satellites will be present to relay voice and data from the lunar surface to an Earth-orbiting satellite. It is also likely that the initial lunar exploration missions will occur in the southern polar region because of interest in the South Pole-Aitken basin (Ref. 10). One potential method of providing high-availability communication to the polar area is to place satellites in highly elliptical orbits (Ref. 11). The elliptical orbital dynamics cause the satellite to remain at apogee for an extended period of time, which provides better visibility than a traditional circular orbit (Fig. 2). In this report, we consider two satellites in a highly elliptical orbital plane over the lunar south pole (Table I).

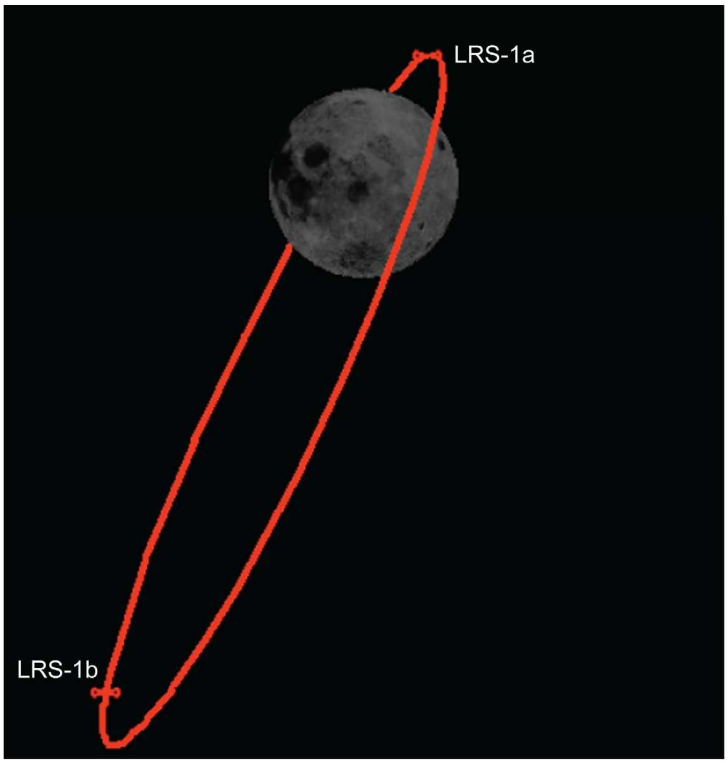

Figure 2.—Highly elliptical lunar orbit. LRS-1a and LRS-1b, Lunar Relay Satellites.

TABLE I.—HIGHLY ELLIPTICAL LUNAR ORBIT PARAMETERS

Constellation	Hybrid elliptical
Satellites	2
Orbital planes	1
Semi-major axis, km	6541.4
Inclination, deg	62.9
Eccentricity	0.6
Radio spectrum	S-band

Similarly, the surface communication architecture remains undefined at this time. Prior publications indicate that it is likely that a communication terminal would be among the first surface architecture elements built on the Moon because of its small cost relative to a satellite (Ref. 9). In addition, it seems reasonable to assume that exploration missions would need a centralized intrasurface architecture. This report considers the case of a 10-m-tall LCT constructed near the lunar habitat.

For this simulation, the radiometric elements (i.e., the LRSs and LCT) each contain a transponder that communicates navigational information using an atomic time and frequency standard. It is necessary that clocks for all of the elements be synchronized to determine a signal propagation delay for calculating pseudorange. One method of accomplishing this is to link all the clocks with an Earth-based operations center through the Tracking and Data Relay Satellite System (TDRSS). This situation could provide a constant mission clock in addition to a navigation time reference.

Another important consideration for the navigation architecture is the communication and processing capability of the radiometric elements. Pseudorange and one-way Doppler measurements can be passively determined from a radio signal. As such, both of these methods are less accurate because of imprecision in the receiver's local oscillator. Range and two-way Doppler measurements require active communication

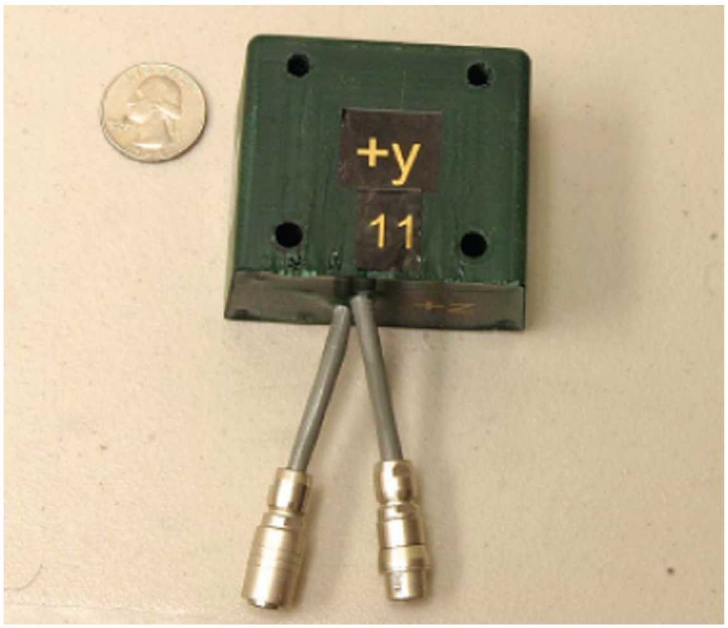

Figure 3.—Microelectromechanical systems (MEMS) inertial measurement unit (IMU) module.

to provide a more accurate distance from the receiver to the radiofrequency source. However, the cost of this accuracy is increased power consumption, since the EVA suit transmitter must be used each time that new position data are requested. In addition, the processing requirements of the LRS and LCT will increase. In this study, we assume that all radiometric elements are capable of two-way operation, but we examine the effect of various one- and two-way combinations on navigational accuracy.

The final component of the proposed lunar navigation architecture is an on-suit microelectromechanical systems (MEMS) inertial unit (Fig. 3). Our simulation considers only one source of IMU data, although that data could be generated from a number of sensors across the EVA suit. The IMU must be capable of providing three-dimensional acceleration measurements that can be double-integrated to arrive at a position change. This technique suffers from inaccuracy because of bias drift; over time, the IMU loses its ability to correctly detect acceleration, such that a randomly varying amount of acceleration is reported even when the actual velocity remains constant. In our approach, we use an EKF to combine radiometrics with inertial measurements, which reduces the impact of this type of error.

Simulation Walking Path

Our simulation defines a surface exploration path beginning near the lunar south pole. Figure 4 shows the starting position of the EVA astronaut and LCT on a two-dimensional projection. The astronaut's trek begins at the lunar habitat and continues northward for 2 hr, for a total walk of 10 km. We chose this distance for consistency with the preliminary Constellation walk-back requirement, and the duration was chosen to yield a realistic travel speed.

Simulated Support Infrastructure

The LCT is placed 250 m east of the habitat to reduce electromagnetic interference. The two LRSs are in a highly elliptical orbit, and both are visible for the entire EVA. The distances between the astronaut and the LRS and LCT are graphed in Figure 5. The sharp dropoff in the LCT range around 4200 sec represents the distance at which the LCT signal is lost.

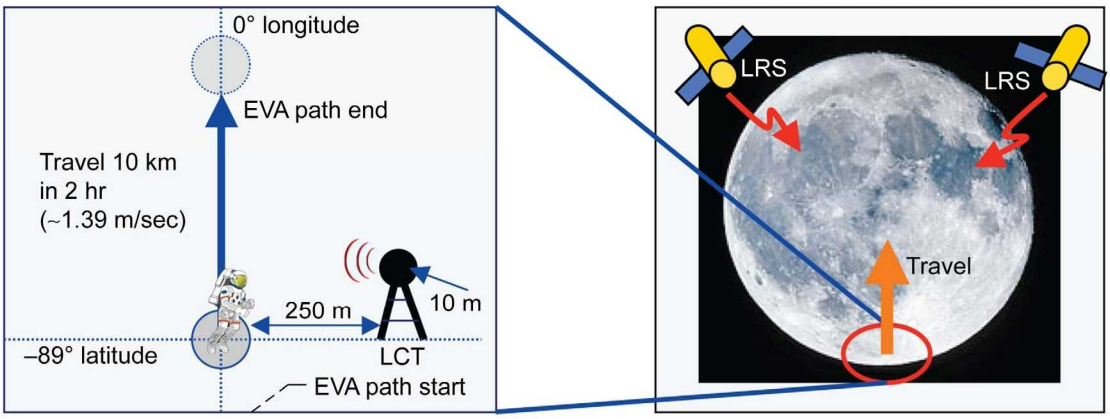

Figure 4.—Simulated extravehicular activity (EVA) path. LCT, Lunar Communication Terminal.

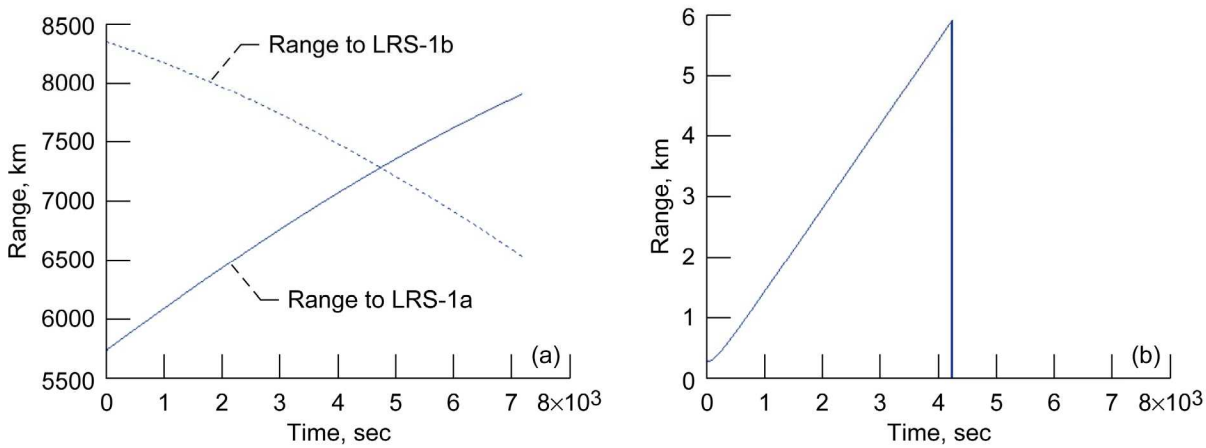

Figure 5.—Range of extravehicular activities (EVAs) to LRSs and LCTs. (a) Range to LRS-1a and LRS-1b. (b) Range to LCT.

EKF Setup and Input Data

The MATLAB simulation uses an EKF to integrate the radiometric and inertial measurements provided by the navigation architecture. Kalman filters in general tend to apply to situations where there is inherent process and measurement noise (Ref. 4). In our case, the radiometric pseudorange and range data are imprecise because of factors such as clock bias and a variable signal-propagation rate. The inertial data similarly suffer from a dynamic acceleration bias that yields a quadratic position error. The goal of the Kalman filter is to provide the best possible system output (here, a specific position on the lunar surface) given a variety of inputs with noncorrelated error. The EKF used in this simulation accomplishes the same purpose for nonlinear systems by calculating new partial derivatives at each iteration of the filter.

TABLE II.—EXTENDED KALMAN FILTER (EKF) STATE TABLE

State	Variable	Definition	Units
1	$\hat{x}_k$ (1)	Latitude	rad
2	$\hat{x}_k$ (2)	Longitude	rad
3	$\hat{x}_k$ (3)	Velocity north	m/sec
4	$\hat{x}_k$ (4)	Velocity east	m/sec
5	$\hat{x}_k$ (5)	Acceleration north	m/sec^2
6	$\hat{x}_k$ (6)	Acceleration east	m/sec^2
7	$\hat{x}_k$ (7)	Clock bias	m
8	$\hat{x}_k$ (8)	Frequency bias	m/sec
9	$\hat{x}_k$ (9)	Acceleration bias north	m/sec^2
10	$\hat{x}_k$ (10)	Acceleration bias east	m/sec^2

The simulation program tracks 10 filter states for each time step of the EVA (Table II). The first six states for position, velocity, and acceleration have a straightforward relationship. The position states are tracked in terms of latitude and longitude, which reduces computational complexity and helps the filter converge to a position fix by restricting travel to points on a spherical lunar model. The program assumes an average lunar radius of 1737.4 km. The seventh state, clock bias, tracks the time drift inaccuracy of the receiver's clock while processing radiometric navigation signals. In essence, this state is represented by Equation (1), where t_{bias} represents the delta between the current time as seen by the transmitter and receiver clocks and c represents the speed of light, used as the signal propagation rate.

The eighth state, frequency bias, is the result of frequency differences between the transmitter and receiver oscillators that lead to inaccuracy when calculating one-way Doppler shift. Finally, the ninth and tenth states track error due to the acceleration bias embedded in the inertial measurements.

$$\hat{x}_k(7) \cong \left(t_{bias}\right)_k c \tag{1}$$

To determine the accuracy of the simulated system, the program generates a baseline state table for each of the 10 states. The information in this table represents the true navigation path to which the EKF should converge over time despite noisy measurements. These states are propagated according to Equation (2), where Rm is the average constant radius of the Moon, rand is an unbounded random number according to the MATLAB *randn* function, and f is the radiometric communication frequency. After the EKF processing is completed, this table is used to determine the filter navigational accuracy.

$$\hat{x}_{k+1} = \begin{bmatrix} 1 & 0 & \frac{1}{Rm} & 0 & 0 & 0 & 0 & 0 & 0 & 0 \\ 0 & 1 & 0 & \frac{1}{Rm\ \cos(\hat{x}_k(1))} & 0 & 0 & 0 & 0 & 0 & 0 \\ 0 & 0 & 1 & 0 & 0 & 0 & 0 & 0 & 0 & 0 \\ 0 & 0 & 0 & 1 & 0 & 0 & 0 & 0 & 0 & 0 \\ 0 & 0 & 0 & 0 & 1 & 0 & 0 & 0 & 0 & 0 \\ 0 & 0 & 0 & 0 & 0 & 1 & 0 & 0 & 0 & 0 \\ 0 & 0 & 0 & 0 & 0 & 0 & 1 & 0 & 0 & 0 \\ 0 & 0 & 0 & 0 & 0 & 0 & 0 & 1 & 0 & 0 \\ 0 & 0 & 0 & 0 & 0 & 0 & 0 & 0 & 1 & 0 \\ 0 & 0 & 0 & 0 & 0 & 0 & 0 & 0 & 0 & 1 \end{bmatrix} \hat{x}_k + \begin{bmatrix} 0 \\ 0 \\ 0 \\ 0 \\ 0 \\ 0 \\ \frac{10\ \text{rand}}{c} \\ \frac{0.01\ \text{rand}}{f\,c} \\ 0 \\ 0 \end{bmatrix} \tag{2}$$

TABLE III.—NOISE COVARIANCE MULTIPLIERS

Two-way Doppler noise covariance, m^2/sec^2	10^{-8}
One-way Doppler noise covariance, m^2/sec^2	10^{-6}
Range noise covariance, m^2/sec^2	1
Pseudorange noise covariance, m^2/sec^2	100
Clock noise covariance, m^2/sec^2	101
Frequency noise covariance, m^2/sec^2	101×10^{-8}
Accelerometer noise covariance, deg^2/sec^4	105×10^{-12}

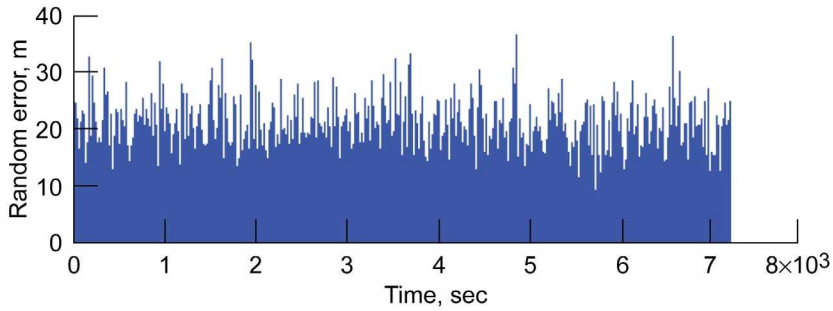

Figure 6.—Random error added to pseudorange measurements.

The satellite orbital position is well-known because the LRS regularly transmits ephemeris data. A radiometric receiver uses this information to produce a pseudorange measurement from the satellite to the current position. The program simulates this process by loading a file containing satellite positions and velocities for the extent of the EVA. By combining this information with the filter's current position estimate (i.e., $\hat{x}_k(1)$ and $\hat{x}_k(2)$), one can calculate pseudorange, range, and one-way and two-way Doppler.

Two versions of the measurement data need to be produced to satisfy the EKF equations. In the first case, the system dynamics are used to predict measurement values. This is simulated by calculating the radiometric values (range, pseudorange, and one-way and two-way Doppler) without any added error. However, in a real-world system, the radiometric receiver produces output that includes the true measurement combined with some additional error inherent to the process. This is simulated in the second case, where a random, normally distributed standard deviation is added to each measurement (Table III). Figure 6 shows an example of the noise added to a typical pseudorange measurement. On average, the simulated values include about 15 m of error.

The IMU acceleration measurements undergo similar processing as the radiometric measurements. The IMU values are easier to simulate because the program models a constant-velocity exploration profile. Acceleration measurements contained in $\hat{x}_k(5)$ and $\hat{x}_k(6)$ consist of the current EKF acceleration estimate added to the accelerometer bias in $\hat{x}_k(9)$ and $\hat{x}_k(10)$. The calculation based on system dynamics is given in Equations (3) and (4), whereas the realistic measurement value is simulated by adding a random normal error to each calculation, where $(y\_accelN)_k$ and $(y\_accelE)_k$ are measurements of acceleration for sample k in the north and east directions, respectively, where k is given in seconds:

$$(y\_\text{accel}N)_k = \hat{x}_k(5) + \hat{x}_k(9) \tag{3}$$

$$(y\_\text{accel}E)_k = \hat{x}_k(6) + \hat{x}_k(10) \tag{4}$$

Once the instrument measurements are simulated, the next step is to generate a series of partial derivatives for each of the measurements in terms of the state variables. Equations (5) to (8) form the basis for this derivation, representing pseudorange pr, range r, one-way Doppler D_1, and two-way Doppler D_2, respectively. In this set of equations, x_e, y_e, and z_e refer to the position of the radiometric

element, and x_r, y_r, and z_r refer to the position of the receiver. Since the calculations are performed with Cartesian coordinates, the receiver position must be converted using Equations (9) to (11). The partial derivatives for acceleration are trivial because the system remains at a constant velocity for the entire EVA. Therefore, the acceleration states are directly related to the accelerometer biases.

$$pr = \sqrt{(x_e - x_r)^2 + (y_e - y_r)^2 + (z_e - z_r)^2} + \hat{x}_k(7) \tag{5}$$

$$r = \sqrt{(x_e - x_r)^2 + (y_e - y_r)^2 + (z_e - z_r)^2} \tag{6}$$

$$D1 = \frac{((x_e - x_r)(\dot{x}_e - \dot{x}_r) + (y_e - y_r)(\dot{y}_e - \dot{y}_r) + (z_e - z_r)(\dot{z}_e - \dot{z}_r))}{\sqrt{(x_e - x_r)^2 + (y_e - y_r)^2 + (z_e - z_r)^2}} + \hat{x}_k(8) \tag{7}$$

$$D2 = \frac{((x_e - x_r)(\dot{x}_e - \dot{x}_r) + (y_e - y_r)(\dot{y}_e - \dot{y}_r) + (z_e - z_r)(\dot{z}_e - \dot{z}_r))}{\sqrt{(x_e - x_r)^2 + (y_e - y_r)^2 + (z_e - z_r)^2}} \tag{8}$$

$$x_r = Rm \cos(\hat{x}_k(1)) \cos(\hat{x}_k(2)) \tag{9}$$

$$y_r = Rm \cos(\hat{x}_k(1)) \sin(\hat{x}_k(2)) \tag{10}$$

$$z_r = Rm \sin(\hat{x}_k(1)) \tag{11}$$

It is important to note that all prior calculations were done in a purely mathematical sense, without regard for the physical limitations of the system. Although it is possible to calculate a range to a satellite on the other side of the Moon, this number has little meaning in the real system because a radiometric signal cannot propagate through the lunar surface. The decision about which data to preserve is made based on the visibility of the navigation element and the system configuration.

Navigational Element Visibility

An angle is computed to determine visibility of the LRS. The modified dot product in Equation (12) is used to calculate the angle to the satellite from the lunar surface, where *ele*_moon is the angle to the lunar satellite as taken from the lunar surface at the receiver, Recv is the current EKF position estimate of the receiver in Cartesian coordinates, SatRecv is a three-dimensional vector pointing from the astronaut's receiver to the satellite, and x, y, and z indicate coordinates. We arbitrarily fixed the minimum elevation at 10°; below this point, it becomes difficult to communicate because of interference from the lunar surface. Also, since the surface is not perfectly flat, this factor allows the simulation to account for diminished visibility while exploring craters, without explicitly defining crater locations. If the calculation reveals that an LRS is not visible from the current receiver location, its measurement data and partial derivatives are discarded and are not passed to the EKF.

$$ele\_moon = 90 - \cos^{-1}\left(\frac{(\mathrm{Recv}) \bullet (\mathrm{SatRecv})}{Rm\sqrt{(\mathrm{SatRecv}_x^2 + \mathrm{SatRecv}_y^2 + \mathrm{SatRecv}_z^2)}}\right)\left(\frac{180}{\pi}\right) \tag{12}$$

A similar equation is used to determine the point at which radiofrequency visibility is lost for the LCT. We assume that the transmission power is adequate to span the entire EVA and that LCT visibility is lost near the horizon. This distance is computed according to Equation (13), where "height" refers to the altitude of the transmitter above the lunar surface. An LCT height of 10 m was selected in this simulation; this implies coverage of approximately 5900 m around the beacon. As with the LRS, the LCT measurements and partial derivatives are discarded once the LCT is no longer visible.

$$\text{horizon} = \sqrt{(2Rm\ \text{height}) + \text{height}^2} \tag{13}$$

EKF Processing

Once the visibility of each navigational element has been assessed, the EKF matrices are assembled using measurement, noise covariance, and partial derivative data for the visible radiometric elements and IMU. Whereas the radiometric elements may drop in and out of view, data from the IMU are always available and incorporated in the filter calculations. For the radiometric elements, the system configuration parameters determine whether one-way or two-way communication is permitted, which determines the correct type of information passed to the EKF. For example, if a particular LRS uses two-way communication, then range, Doppler, clock bias, and frequency bias are known definitively. However, the one-way elements are restricted to providing only pseudorange and one-way Doppler information to the EKF, even though the other types of data were calculated earlier. This is done to better reflect the operational environment; we can determine items such as range mathematically, but this is not possible for a real system that uses one-way communication.

The propagation of covariances and states between time steps are handled according to the standard EKF equations (Eqs. (14) to (20)) as discussed in Reference 12. The governing state equation of the problem is defined as

$$\hat{x}_k^- = f_{k-1}\left(\hat{x}_{k-1}^+, u_{k-1}, 0\right) \tag{14}$$

where $\hat{x}_k^-$ is the state table for time step k before filtering is performed, f_{k-1} is a discrete function linking time step k to the previous time step, and u_{k-1} is the control variable.

The equation that defines the radiometric and inertial measurements is

$$y_k = h_k\left(\hat{x}_k, 0\right) \tag{15}$$

where y_k represents the measurements for the current time step (e.g., range and acceleration) and h_k is a discrete function linking the measurements to state $\hat{x}_k$. It follows that the EKF covariance can be propagated from state to state according to

$$P_k^- = F_{k-1}P_{k-1}^+F_{k-1}^T + Q_{k-1} \qquad F_{k-1} = \left.\frac{\partial f_{k-1}}{\partial x}\right|_{\hat{x}_{k-1}^+} \tag{16}$$

where P_k is the covariance matrix for each state in time step k, F_{k-1} is the partial derivative matrix of f in terms of the state table x for the previous time step, and Q_{k-1} is the covariance values for the normally distributed process noise associated with the states. The Kalman gain, which determines the influence that the measurement values have on the change in state values, is calculated as

$$K_k = P_k^- H_k^T\left(H_k P_k^- H_k^T + R_k\right)^{-1} \qquad H_k = \left.\frac{\partial h_k}{\partial x}\right|_{\hat{x}_k^-} \tag{17}$$

where K_k is the Kalman gain, H_k is the partial derivative matrix of the measurements in terms of the state table, and R_k is the covariance matrix for the normally distributed measurement noise. It then follows that the state table is propagated according to

$$\hat{x}_k^+ = \hat{x}_k^- + K_k\left(y_k - h_k\left(\hat{x}_k^-, 0\right)\right) \tag{18}$$

and the covariance matrix is propagated by

$$P_k^+ = (I - K_k H_k) P_k^- (I - K_k H_k)^T + K_k R_k K_k^T \tag{19}$$

to complete the EKF iteration, where I is the identity matrix. At the beginning of the next time step for the same 2-hr EVA period, the filter states are propagated forward according to

$$\hat{x}_{k+1}^- = \begin{bmatrix} 1 & 0 & \frac{1}{Rm} & 0 & 0 & 0 & 0 & 0 & 0 & 0 \\ 0 & 1 & 0 & \frac{1}{Rm\cos(\hat{x}_k(1))} & 0 & 0 & 0 & 0 & 0 & 0 \\ 0 & 0 & 1 & 0 & 0 & 0 & 0 & 0 & 0 & 0 \\ 0 & 0 & 0 & 1 & 0 & 0 & 0 & 0 & 0 & 0 \\ 0 & 0 & 0 & 0 & 1 & 0 & 0 & 0 & 0 & 0 \\ 0 & 0 & 0 & 0 & 0 & 1 & 0 & 0 & 0 & 0 \\ 0 & 0 & 0 & 0 & 0 & 0 & 1 & 0 & 0 & 0 \\ 0 & 0 & 0 & 0 & 0 & 0 & 0 & 1 & 0 & 0 \\ 0 & 0 & 0 & 0 & 0 & 0 & 0 & 0 & 1 & 0 \\ 0 & 0 & 0 & 0 & 0 & 0 & 0 & 0 & 0 & 1 \end{bmatrix} \hat{x}_k^+ \tag{20}$$

The step in Equation (20) is performed a priori, or without influence from measurements, since the EKF attempts to develop an internal prediction of the next state based on the governing equations. After propagating the state table, the program computes new random noise values and loops to the point where measurement values (e.g., pseudorange, Doppler, and acceleration) are generated.

Once a 2-hr period is complete, several noise runs are performed for the same period. This allows different random walk characteristics to be observed and helps to provide bounds on the possible navigation error. After computing several solutions for the same EVA period, the program loads new satellite position and velocity data for the next period, and all measurements are repeated.

Position Error Results

We determine the performance of the lunar navigational system by comparing the root sum squares of the EKF and baseline position data for the extent of the EVA. After converting the latitude and longitude position states to Cartesian coordinates, an error is generated for each time step according to

$$\mathrm{err}_k = \sqrt{(X_{\mathrm{base}} - X_{\mathrm{EKF}})_k^2 + (Y_{\mathrm{base}} - Y_{\mathrm{EKF}})_k^2 + (Z_{\mathrm{base}} - Z_{\mathrm{EKF}})_k^2} \tag{21}$$

where err_k is the overall position error in meters, X_{base}, Y_{base}, and Z_{base} are the baseline position coordinates for time step k, and X_{EKF}, Y_{EKF}, and Z_{EKF} are the coordinates determined by the EKF for the same time step. This error determination is repeated for each time step in the EVA, and then repeated again for each random walk of the EVA for the same time period.

Figures 7 to 14 show the results for several system configurations. The simulations included 30 random walks over the same 2-hr EVA period, with an initial 100-m uncertainty in the starting position. The source of two-way range and Doppler measurements was varied between figures to demonstrate how different system configurations affect the navigational accuracy and convergence time. The experimental configurations are given in Table IV.

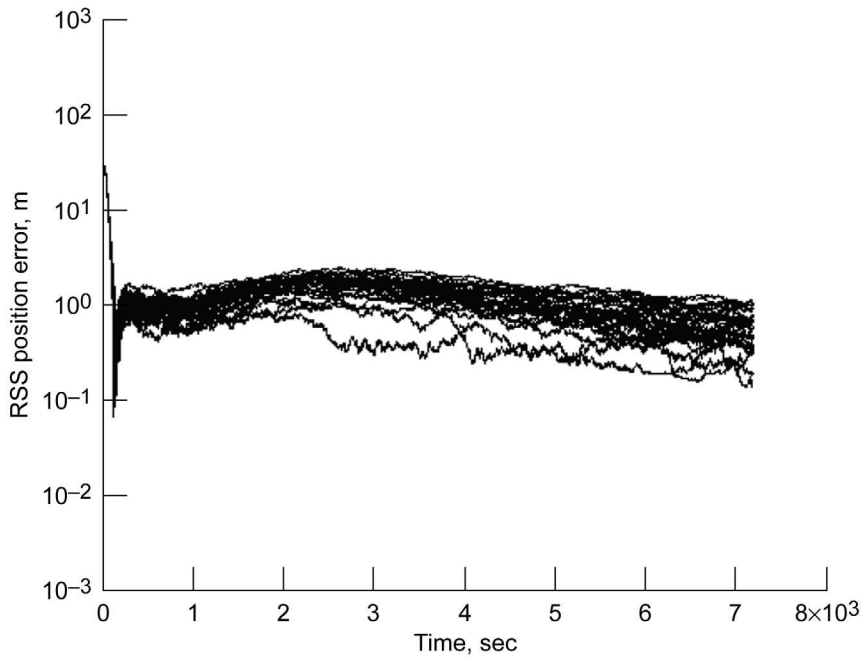

Figure 7.—Position error with LRS-1a using two-way communication. RSS, root-sum-square.

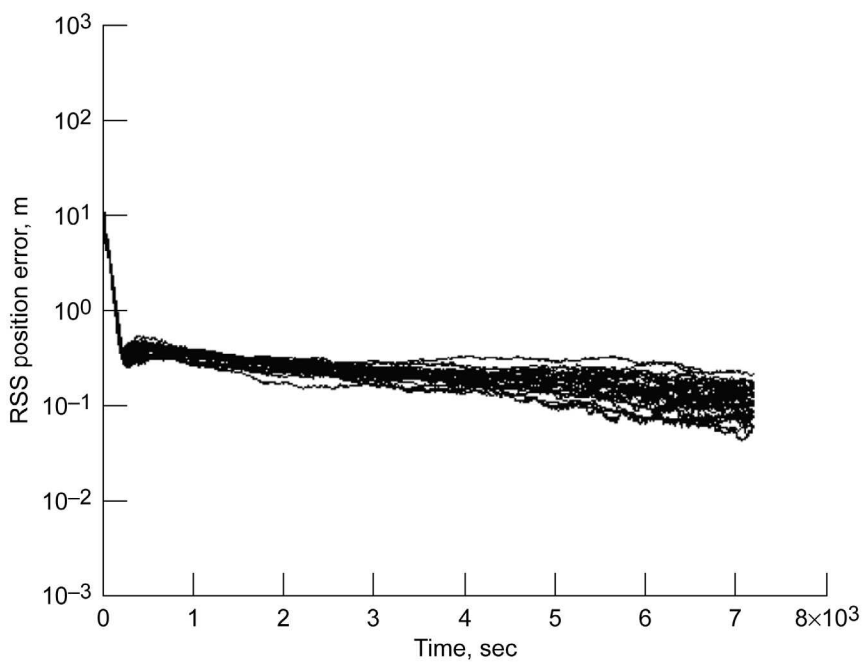

Figure 8.—Position error with LRS-1b using two-way communication.

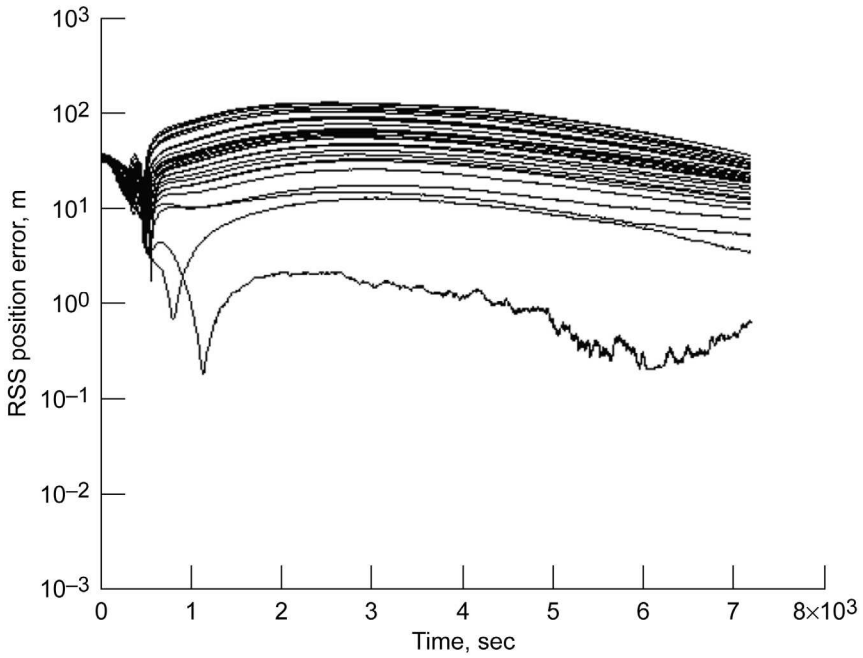

Figure 9.—Position error with LCT using two-way communication.

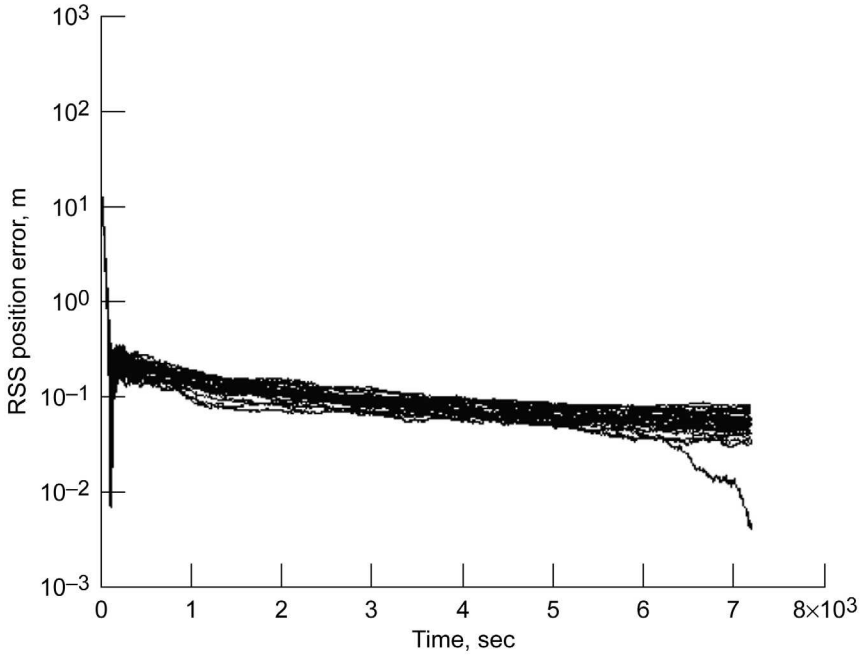

Figure 10.—Position error with LRS-1a and LRS-1b using two-way communication.

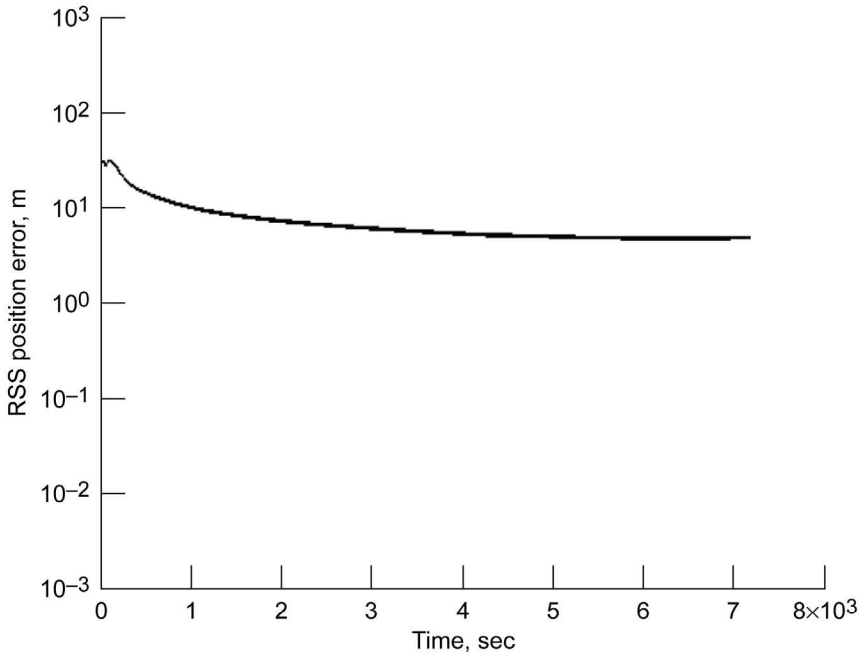

Figure 11.—Position error with LRS-1b and LCT using two-way communication.

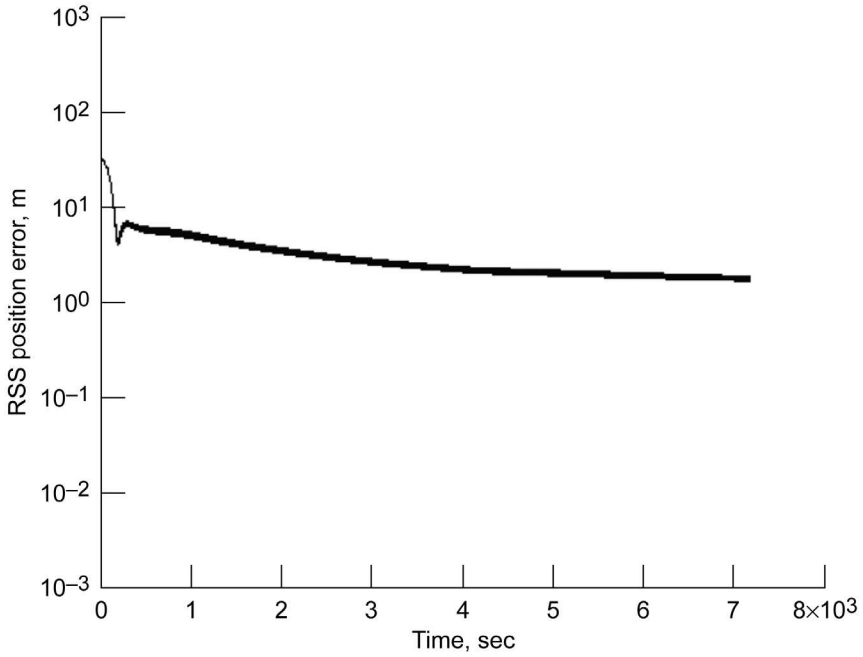

Figure 12.—Position error with LRS-1a and LCT using two-way communication.

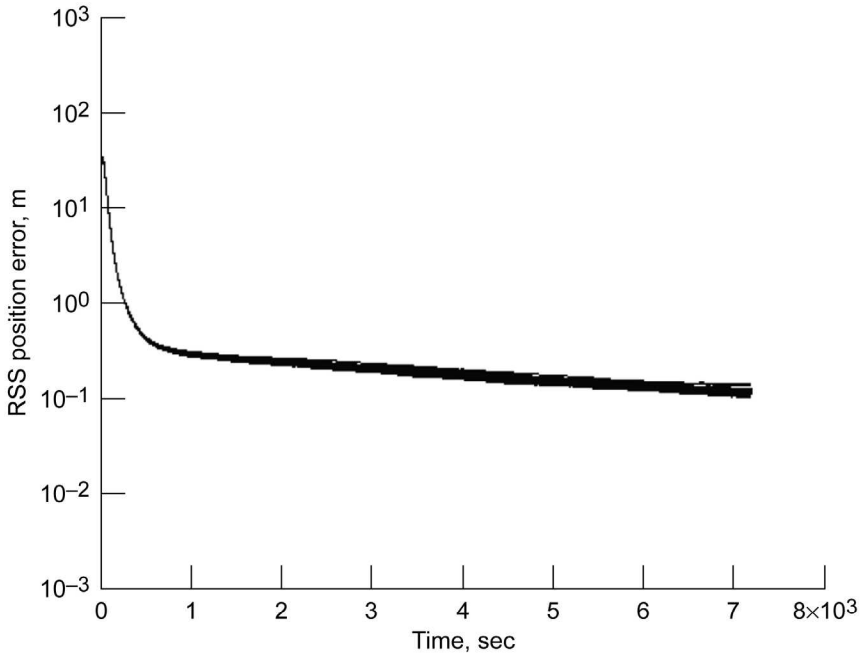

Figure 13.—Position error with all elements using two-way communication.

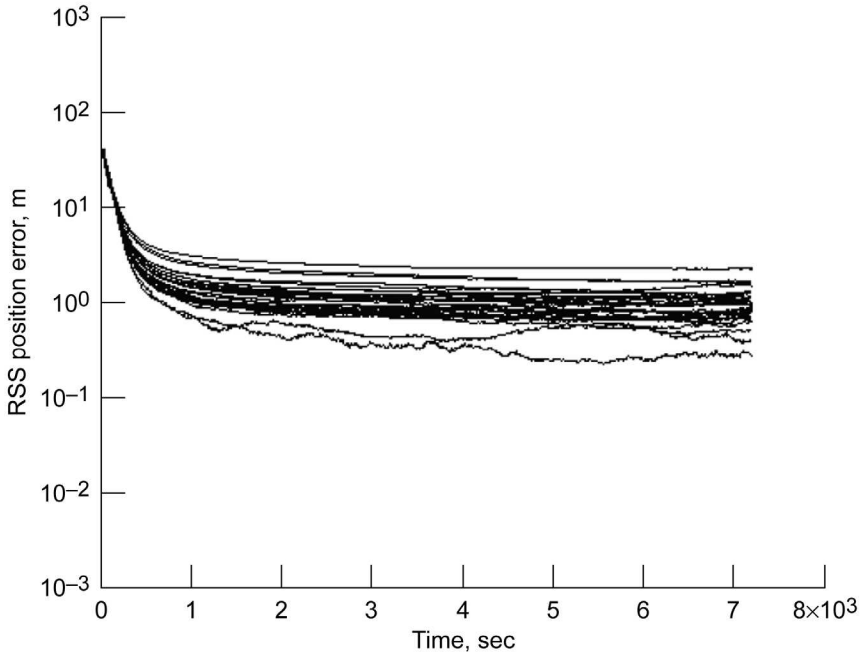

Figure 14.—Position error with all elements using one-way communication.

TABLE IV.—EXPERIMENTAL CONFIGURATIONS[a]

Figure	LRS-1a	LRS-1b	LCT	IMU
7	Two-way	One-way	One-way	Present
8	One-way	Two-way	One-way	Present
9	One-way	One-way	Two-way	Present
10	Two-way	Two-way	One-way	Present
11	One-way	Two-way	Two-way	Present
12	Two-way	One-way	Two-way	Present
13	Two-way	Two-way	Two-way	Present
14	One-way	One-way	One-way	Present

[a]LRS, Lunar Relay Satellite; LCT, Lunar Communication Terminal; IMU, inertial measurement unit.

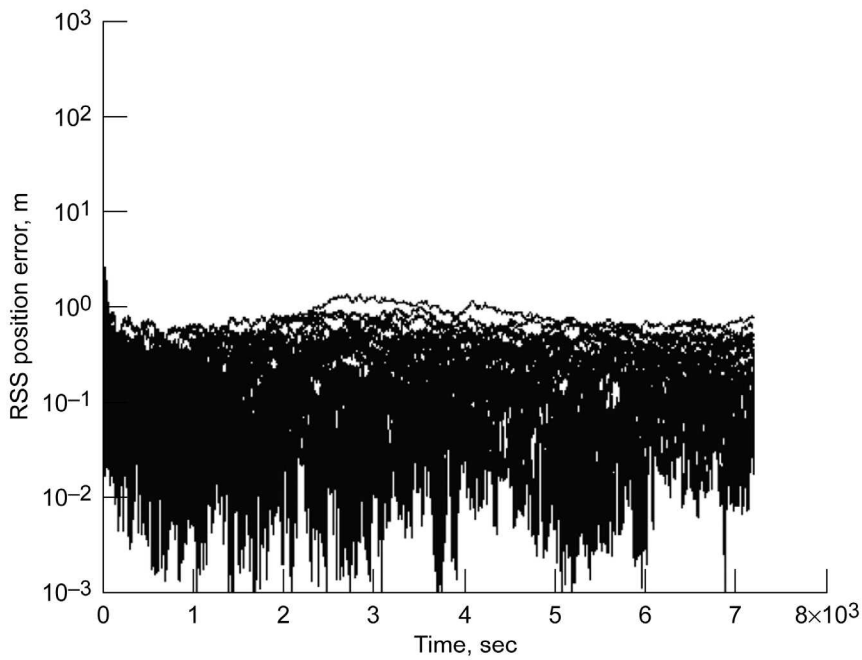

Figure 15.—Position error with 10-m initial uncertainty.

Figures 15 to 18 show the effect of changing the initial position state and covariance data for the EKF. Each graph displays the navigational position error for the corresponding initial position error. For these figures, the system uses two-way communication with LRS-1a and one-way communication with LRS-1b and the LCT. The starting position is offset by 10, 50, 200, and 500 m in Figures 15, 16, 17, and 18, respectively. This represents uncertainty in the initial position, which tends to delay filter convergence.

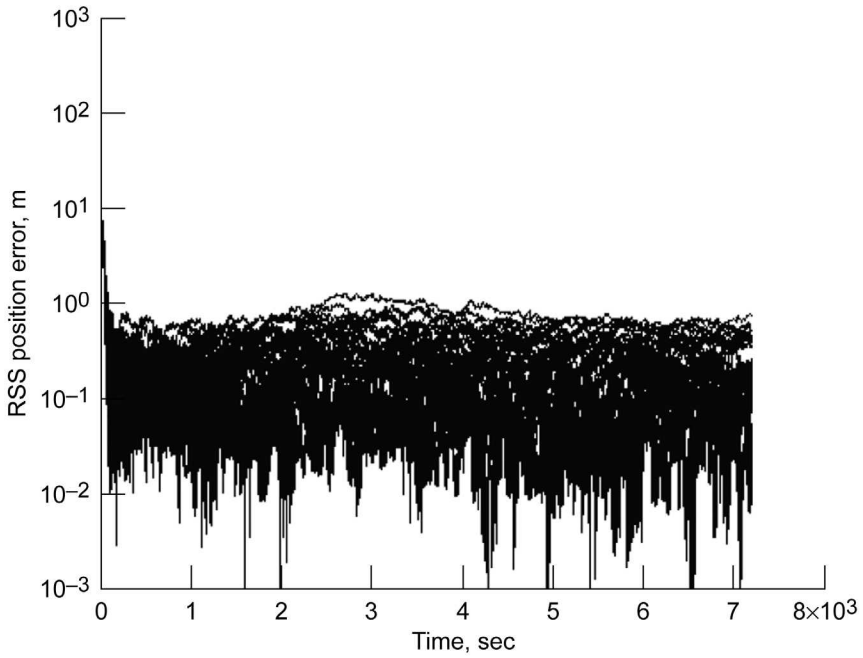

Figure 16.—Position error with 50-m initial uncertainty.

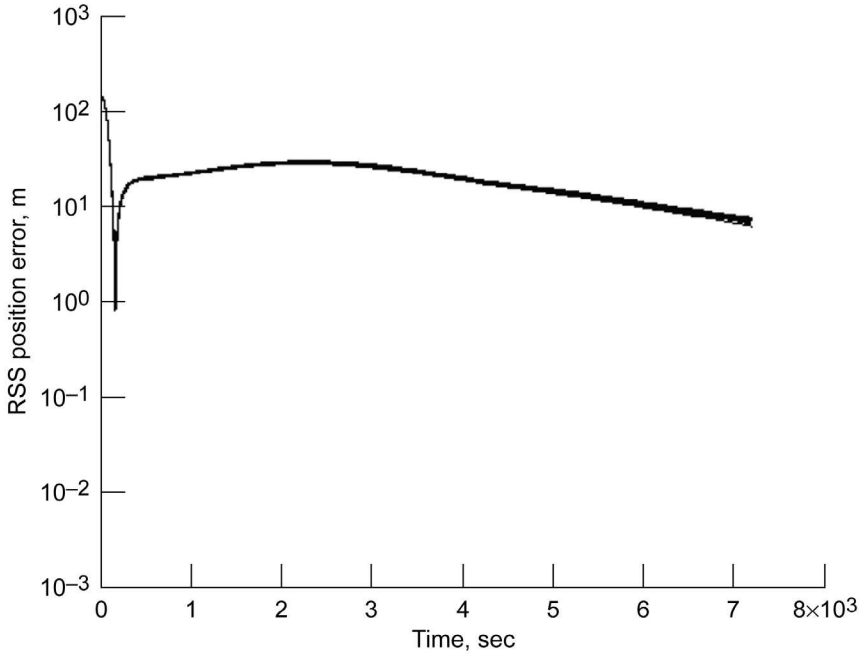

Figure 17.—Position error with 200-m initial uncertainty.

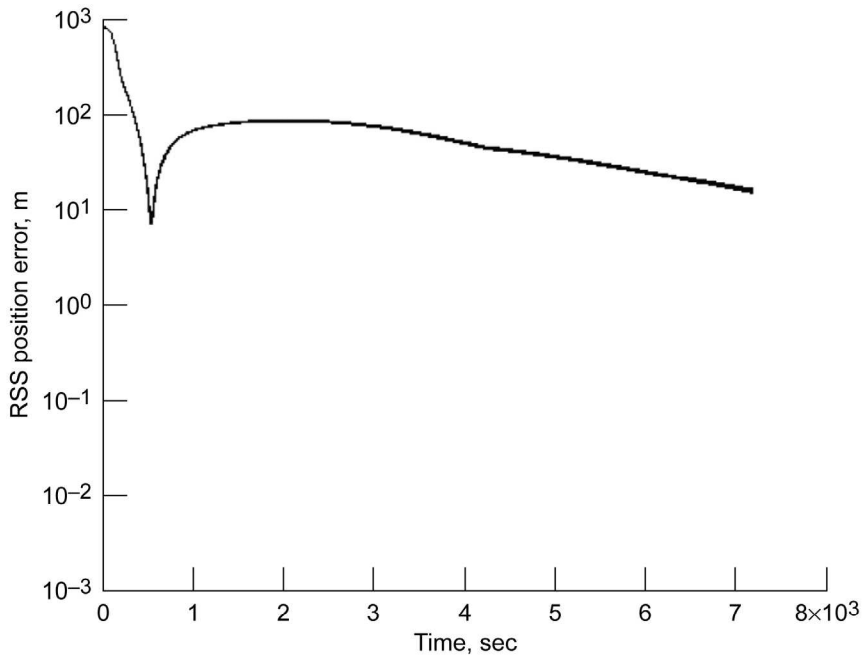

Figure 18.—Position error with 500-m initial uncertainty.

Figures 19 to 22 show the effect of reducing the number of radiometric elements available. Since the lunar navigation architecture remains uncertain, these charts demonstrate the type of accuracy possible given fewer elements than expected. With the assumption that LRS-1b is not present, Figure 19 shows the navigation accuracy when LRS-1a is used for two-way communication and the LCT is used for one-way communication. Figure 20 displays one-way communication for LRS-1a and the LCT. In Figures 21 and 22, no LRS is present and the LCT performs two-way and one-way communication, respectively.

Figure 23 presents an IMU-only configuration. In this case, no radiometric elements are considered in the EKF, and only the inertial data are processed.

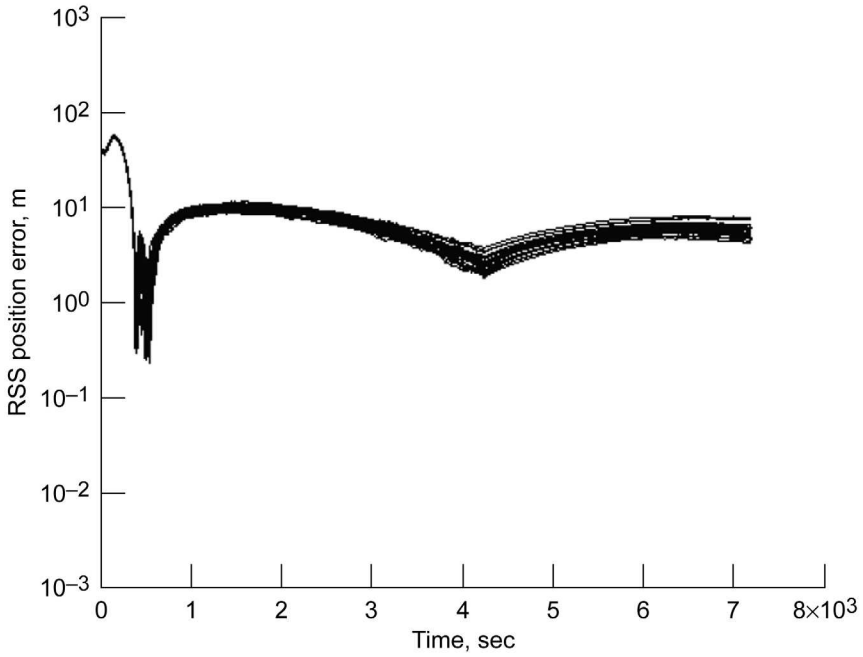

Figure 19.—Position error with LRS-1a using two-way communication, LRS-1b not present, and LCT using one-way communication.

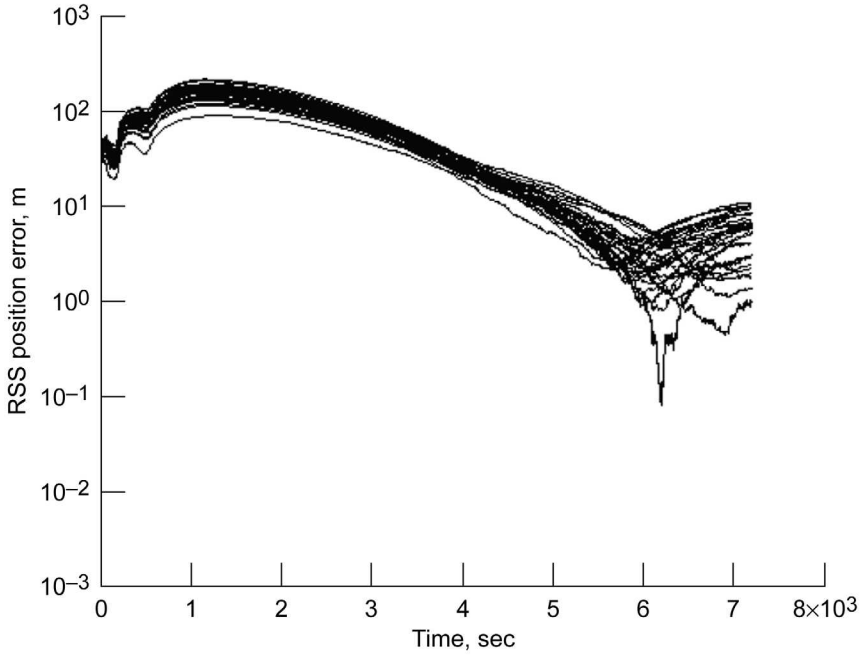

Figure 20.—Position error with LRS-1a using one-way communication, LRS-1b not present, and LCT using one-way communication.

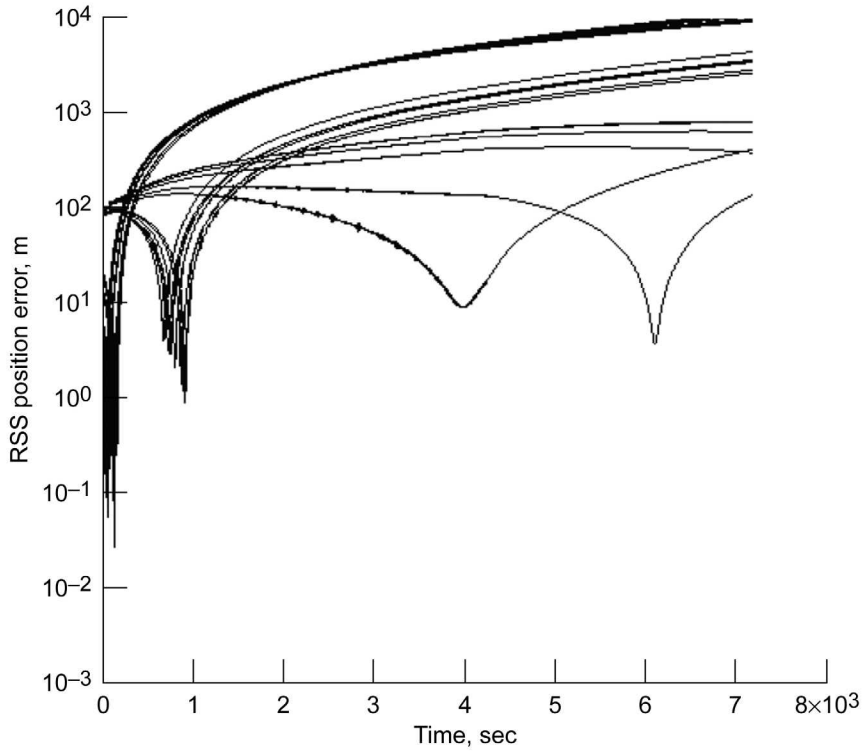

Figure 21.—Position error with no LRS present and LCT using two-way communication.

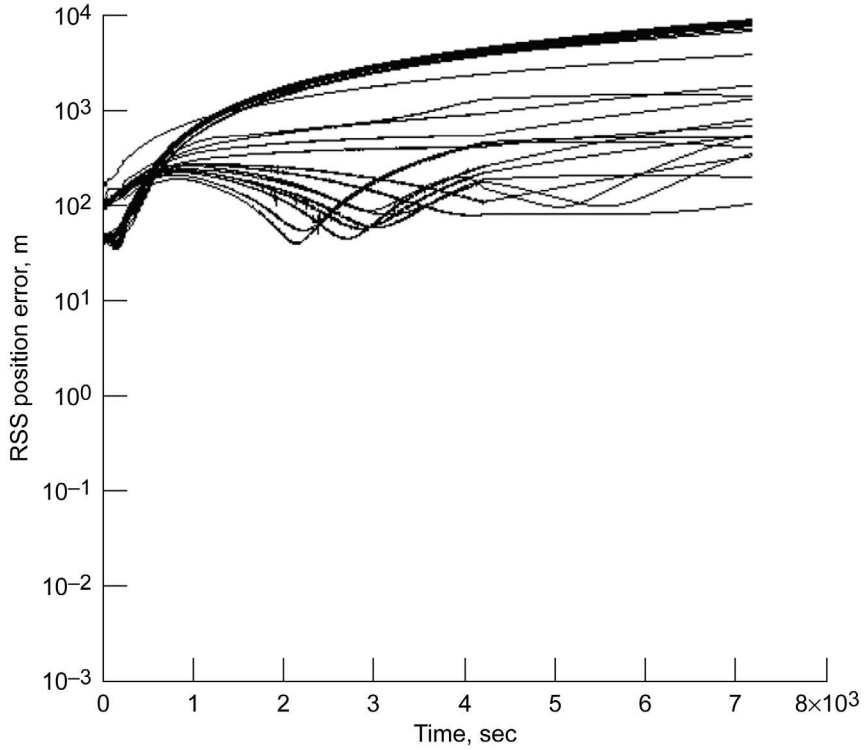

Figure 22.—Position error with no LRS present and LCT using one-way communication.

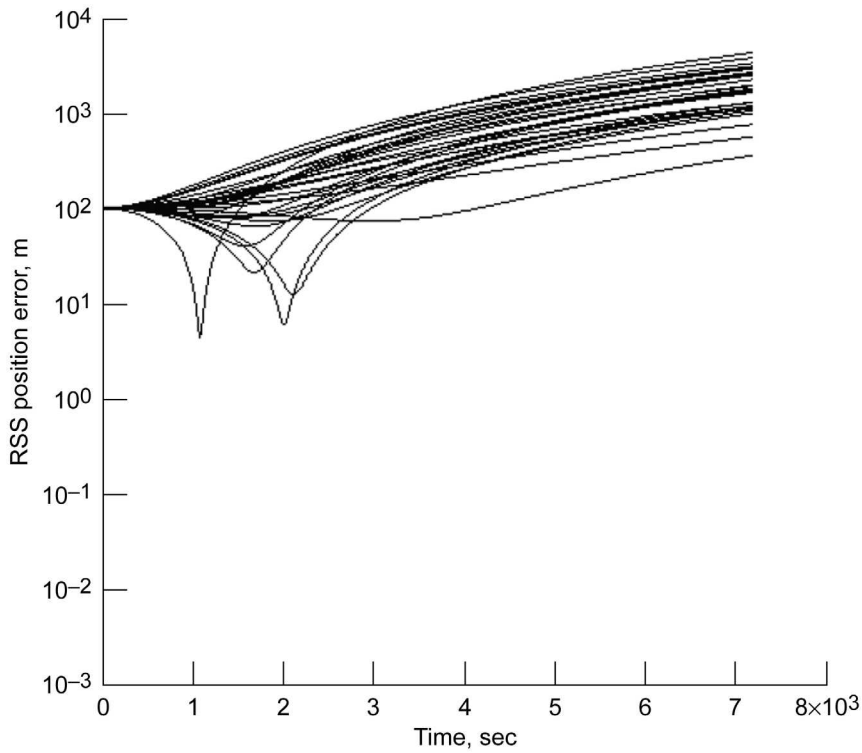

Figure 23.—Position error with inertial measurement unit only.

Discussion

The system configuration tests in Figures 7 to 14 illustrate the importance of finding a balance between the number of one-way and two-way radiometric elements. The best and most consistent result was obtained in Figure 13, where navigational accuracy converged to less than 1 m within 5 min. In this case, all radiometric elements operated in two-way mode. However, the results obtained in Figures 8 and 10 are similar, with the exception that the navigation path tends to be subject to greater influence from the random walk effect. The Figure 8 test assumed that LRS-1b was the only radiometric element performing two-way communication, so this setup would deliver the greatest mix of performance and energy savings. However, it is notable that the same level of accuracy is not obtainable when LRS-1a is in the same situation (Fig. 7), so there is likely a correlation between satellite position and accuracy. Taking this into account, a more consistent result is obtained when both LRSs use two-way communication (Fig. 10).

As one would expect, the initial position tests reveal that performance is somewhat dependent on the accuracy of the starting position. When comparing Figures 15 and 16, it is not clear that initial accuracy between 10 and 50 m has a significant performance impact. Even when the error increased 100 m, as in Figure 7, the filter output was accurate to within 3 m for the entire EVA. As the initial position uncertainty increased to 200 and 500 m in Figures 17 and 18, accuracy decreased to approximately 20 and 100 m in 5 min, respectively.

The effect of eliminating one or more radiometric elements was a pronounced decrease in the system accuracy. A comparison of Figures 7 and 19 shows that the system accuracy is reduced from 1 m in 5 min to 10 m in 5 min when LRS-1b is eliminated. Accuracy decreases significantly by a factor of 10 between Figures 19 and 20 when the remaining LRS-1a is changed to one-way communication. When no LRS was used, the EKF appeared to fail to converge, generating a position error greater than 1 km.

When all radiometric elements were eliminated and the IMU was the sole source of navigation data, performance suffered drastically. The filter did not converge, yielding a position error greater than 1 km over the EVA. The simulated navigation profile remained at a constant velocity, so ideally the IMU had no acceleration to report for the EVA. However, this was not the case because of drift in the acceleration bias. As the EVA duration increased, errors contributed by the IMU also increased.

Conclusions

This report presented one possible system architecture for lunar surface navigation and analyzed various configuration options in terms of their navigational error. It appears that the navigation system will yield its best performance when two-way satellite communication is available between the radiometric receiver and the Lunar Relay Satellite. In this case, an accuracy of less than 1-m error within 5 min is attainable. The system is responsive to uncertainty in the initial starting position of the radiometric receiver, although significant performance loss was observed only for initial errors greater than 100 m. The navigational accuracy experienced a 100 times degradation by the loss of one satellite; however, this impact was mitigated by a factor of 10 if the remaining satellite could perform two-way communication. The extended Kalman filter (EKF) responded poorly to the situation where a Lunar Communication Terminal was the only radiometric element and even worse when the IMU was used alone, without radiometric support.

The combination of radiometrics and inertial measurements using an EKF is viable for applications to lunar surface navigation. The presented results demonstrate the feasibility of determining a position to within 1-m accuracy in 5 min.

Future Work

The program has some limitations that may affect its accuracy. Most notably, the use of latitude and longitude for position data implies a constant lunar radius. The significance of this factor must be analyzed further to determine the impact of exploring lunar craters or hills. One possible approach is to convert the program to a Cartesian coordinate system, though this may reduce filter convergence.

The exploration profile discussed in this report only considers a constant velocity walk-back profile. To better understand the impact of the inertial measurement unit on the navigational system accuracy, a situation involving a changing velocity needs to be considered. Although the IMU only contributed error in this simulation, it may prove more valuable in situations where a fine measurement granularity is needed between radiometric data.

Appendix—Symbols

c	speed of light
D_1	one-way Doppler
D_2	two-way Doppler
*ele*_moon	elevation of a radiometric element viewed from the lunar surface
err_k	overall position error in meters
F_{k-1}	partial derivative matrix of f in terms of the state table x for the previous time step
f	radiometric communication frequency
f_{k-1}	discrete function linking time step k to the previous time step
H_k	partial derivative matrix of the measurements in terms of the state table
h_k	discrete function linking the measurements to state $\hat{x}_k$
I	identity matrix
K_k	Kalman gain
P_k	covariance matrix for each state in time step k
pr	pseudorange
Q_{k-1}	covariance values for the normally distributed process noise associated with the states
R_k	covariance matrix for the normally distributed measurement noise
Rm	average constant radius of the Moon
r	range
rand	unbounded random number according to the MATLAB *randn* function
Recv	current EKF position estimate of the receiver in Cartesian coordinates
SatRecv	vector from the receiver to the satellite
t_{bias}	delta between the current time as seen by the transmitter and receiver clocks
u_{k-1}	control variable
X_{base}, Y_{base}, Z_{base}	baseline position coordinates for time step k
X_{EKF}, Y_{EKF}, Z_{EKF}	coordinates determined by the EKF for the same time step
x_e, y_e, z_e	position coordinates of the radiometric element
$\dot{x}_e$, $\dot{y}_e$, $\dot{z}_e$	velocity coordinates of the radiometric element ($\dot{x}_e = [\mathrm{d}(x_e)]/\mathrm{d}t$, etc.)
x_r, y_r, z_r	position coordinates of the receiver
$\dot{x}_r$, $\dot{y}_r$, $\dot{z}_r$	velocity of the receiver
$\hat{x}_k$	filter state variable

$\hat{x}_k^-$	state table for time step k before filtering is performed
y_k	measurements for the current time step (e.g., range and acceleration)
$(y\_\text{accel}N)_k$	measurement of northward acceleration
$(y\_\text{accel}E)_k$	measurement of eastward acceleration

References

1. Daly, P.: Navstar GPS and GLONASS: Global Satellite Navigation Systems. Electron. Commun. Engrg. J., vol. 5, issue 6, Dec. 1993, pp. 349–357.
2. Bar-Itzhack, I.Y.; and Carothers, M.L.: LRV Navigation Support at Bellcomm During the Apollo 15 Mission—Case 320. Bellcomm Memorandum B71 08026, Aug. 19, 1971. http://hdl.handle.net/2060/19790072562
3. Constellation Architecture Requirements Document (CARD). CxP 70000, Rev. B, Feb. 13, 2008. http://www.everyspec.com/NASA/NASA+-+CxP+PUBS/download.php?spec=CxP_70000_CARD_RevB.005804.pdf
4. Simon, Dan: Optimal State Estimation: Kalman, H Infinity, and Nonlinear Approaches. Wiley & Sons, 2006.
5. Honghui, Qi; and Moore, J.B.: Direct Kalman Filtering Approach for GPS/INS Integration. Aerospace and Electronic Systems, IEEE Trans., vol. 38, issue 2, 2002, pp. 687–693.
6. Scherzinger, Bruno M.; and Woolven, Steven: POS/MV—Handling GPS Outages With Tightly Coupled Inertial/GPS Integration. OCEANS '96, MTS/IEEE, Prospects for the 21st Century, Conference Proceedings, vol. 1, 1996, pp. 422–428.
7. Lipp, Wolfgang; Sagrestani, Vicenzo; and Sarrica, Rosario: Integrated GPS/Fibre Optic Gyro Land Navigation System. Position Location and Navigation Symposium, 1994, IEEE, 1994, pp. 447–452.
8. Call, Curt, et al.: Performance of Honeywell's Inertial/GPS Hybrid (HIGH) for RNP Operations. Position, Location, and Navigation Symposium, 2006 IEEE/ION, 2006.
9. Bhasin, Kul B.; Warner, Joseph D.; and Anderson, Lynn M.: Lunar Communication Terminals for NASA Exploration Missions: Needs, Operations Concepts, and Architectures. International Communications Satellite Systems Conference, 2008.
10. David, Leonard: Lunar South Pole Landing Sites Studied. Space.Com, Imaginova Corp., 2003. http://www.space.com/missionlaunches/moon_southpole_030604.html
11. Ely, Todd: Stable Constellations of Frozen Elliptical Lunar Orbits. J. Astronautical Sci., vol. 53, no. 3, 2005, pp. 301–316.
12. Lemon, Kimber; and Welch, Bryan W.: Comparison of Nonlinear Filtering Techniques for Lunar Surface Roving Navigation. NASA/TM—2008-215152, 2008. http://gltrs.grc.nasa.gov

REPORT DOCUMENTATION PAGE	Form Approved OMB No. 0704-0188

1. REPORT DATE *(DD-MM-YYYY)* 01-06-2009	**2. REPORT TYPE** Technical Memorandum	**3. DATES COVERED** *(From - To)*
4. TITLE AND SUBTITLE A Kalman Approach to Lunar Surface Navigation Using Radiometric and Inertial Measurements		**5a. CONTRACT NUMBER** **5b. GRANT NUMBER** **5c. PROGRAM ELEMENT NUMBER**
6. AUTHOR(S) Chelmins, David, T.; Welch, Bryan, W.; Sands, O., Scott; Nguyen, Binh, V.		**5d. PROJECT NUMBER** **5e. TASK NUMBER** **5f. WORK UNIT NUMBER** WBS 903184.04.03.02.02
7. PERFORMING ORGANIZATION NAME(S) AND ADDRESS(ES) National Aeronautics and Space Administration John H. Glenn Research Center at Lewis Field Cleveland, Ohio 44135-3191		**8. PERFORMING ORGANIZATION REPORT NUMBER** E-16883
9. SPONSORING/MONITORING AGENCY NAME(S) AND ADDRESS(ES) National Aeronautics and Space Administration Washington, DC 20546-0001		**10. SPONSORING/MONITOR'S ACRONYM(S)** NASA **11. SPONSORING/MONITORING REPORT NUMBER** NASA/TM-2009-215593

12. DISTRIBUTION/AVAILABILITY STATEMENT
Unclassified-Unlimited
Subject Category: 17
Available electronically at http://gltrs.grc.nasa.gov
This publication is available from the NASA Center for AeroSpace Information, 301-621-0390

13. SUPPLEMENTARY NOTES

14. ABSTRACT
Future lunar missions supporting the NASA Vision for Space Exploration will rely on a surface navigation system to determine astronaut position, guide exploration, and return safely to the lunar habitat. In this report, we investigate one potential architecture for surface navigation, using an extended Kalman filter to integrate radiometric and inertial measurements. We present a possible infrastructure to support this technique, and we examine an approach to simulating navigational accuracy based on several different system configurations. The results show that position error can be reduced to 1 m after 5 min of processing, given two satellites, one surface communication terminal, and knowledge of the starting position to within 100 m.

15. SUBJECT TERMS
Moon; Navigation; Lunar surface; Surface navigation; Radio navigation; Satellite navigation; Systems; Positioning

16. SECURITY CLASSIFICATION OF:			**17. LIMITATION OF ABSTRACT**	**18. NUMBER OF PAGES**	**19a. NAME OF RESPONSIBLE PERSON**
a. REPORT	**b. ABSTRACT**	**c. THIS PAGE**			STI Help Desk (email:help@sti.nasa.gov)
U	U	U	UU	30	**19b. TELEPHONE NUMBER** *(include area code)* 301-621-0390

Standard Form 298 (Rev. 8-98)
Prescribed by ANSI Std. Z39-18